

# Energy release rate of the fiber/matrix interface crack growth in $[0_{m \cdot 2l}^{\circ}, 90_l^{\circ}]_S$ laminates under transverse loading: effect of $0^{\circ}/90^{\circ}$ interface

Luca Di Stasio<sup>a,b</sup>, Janis Varna<sup>a</sup>, Zoubir Ayadi<sup>b</sup>

<sup>a</sup>Luleå University of Technology, University Campus, SE-97187 Luleå, Sweden

<sup>b</sup>Université de Lorraine, EEIGM, IJL, 6 Rue Bastien Lepage, F-54010 Nancy, France

---

## Abstract

Models of Representative Volume Elements (RVEs) of cross-ply  $[0_{m \cdot 2l}^{\circ}, 90_l^{\circ}]_S$  laminates with different geometric configurations and damage states are studied. Debond growth is characterized by the estimation of the Mode I and Mode II Energy Release Rate (ERR) using the Virtual Crack Closure Technique (VCCT) and the J-integral. It is found that the presence of the  $0^{\circ}/90^{\circ}$  interface and the thickness of the  $0^{\circ}$  layer have no effect, apart from laminates with *ultra-thin*  $90^{\circ}$  plies where it is however modest. With the exception of cross-ply laminates with an *ultra-thin*  $90^{\circ}$  ply, no difference is found in debond ERR between a UD composite and a cross-ply laminate.

**Keywords:** Polymer-matrix Composites (PMCs), Thin-ply, Transverse Failure, Debonding, Finite Element Analysis (FEA)

---

## 1. Introduction

Since the development of the *spread tow* technology or “FUKUI method” [1, 2], significant efforts have been directed toward the characterization of *thin-ply* laminates [3, 4, 5, 6, 7, 8, 9, 10, 11, 12, 13, 14, 15] and their application to mission-critical structures in the aerospace sector [16, 17, 18, 19].

At the lamina level, the use of *thin-ply*s leads to more regular and homogeneous microstructures [9, 12]. Measurements of ply level properties (tensile and compressive modulus, Poisson’s ratio, ultimate tensile strength, tensile on-

set of damage, interlaminar shear strength) on UD specimens ( $[0_m^\circ]$  and  $[90_m^\circ]$ )  
10 revealed no remarkable difference with average properties available in the literature for the same type of fiber, nor showed any particular dependence on the ply thickness [12]. Only an increase of the ultimate compressive strength in the fiber direction was observed with very thin plies ( $\sim 4$  fiber diameters), although with very scattered values, which the authors claim to be due to the  
15 fiber arrangement's increased regularity which prevents the onset of fiber microbuckling [12]. A number of researchers [4, 5, 6, 7] has reported improvements in fatigue life with the use of *thin-ply*s, which are explained as a consequence of delayed propagation of free edge delaminations and intralaminar cracks. Several researchers have analyzed the effect of *thin-ply*s on damage development  
20 under static [3, 6, 7, 8, 9, 10, 11, 12], fatigue [4, 6, 7, 8, 12] and impact loadings [6, 7, 8, 12]. It seems apparent that *thin-ply* laminates possess an increased ability to delay, and in some cases even suppress, the onset and propagation of intralaminar cracks (or transverse or matrix or micro-cracks).

The first appearance of transverse cracks is known to be characterized by the  
25 occurrence of fiber/matrix interface cracks (also referred to as debonds), which grow along the fiber arc direction, then kink out of the interface and coalesce forming a transverse crack [20]. Different approaches have been applied to model the initiation and growth of debonds. The Cohesive Zone Model (CZM) has been used to mimic the propagation of debonds along fiber interfaces; coupled with a failure criterion for the matrix, it has provided simulations of the  
30 growth of transverse cracks starting from a virgin material [21, 22, 23, 24]. The main advantages of this approach are the possibility to observe the development of a simulated crack path and to record a load-displacement curve to compare with experimental measurement. However, various observations cast a doubt  
35 about the applicability of the CZM: the bi- (for 2D models) and tri- (in 3D) axially of the matrix stress state in the inter-fiber region that is linked with a cavitation-like failure of the polymer [25]; the locality and mode dependency of the interface failure [26]; the problematic use at the microscopic level of properties measured in UD specimens at the laminate level [22]. A second approach

40 that obviates these drawbacks is the application of Linear Elastic Fracture Me-  
 chanics (LEFM) arguments to the study of debond growth. The analysis focuses  
 on the evaluation of Mode I and Mode II Energy Release Rate (ERR) at the  
 crack tip by means of the Virtual Crack Closure Technique (VCCT) [27] or the  
 J-Integral method [28]. The stress and strain field, required for the ERR compu-  
 45 tation, can be solved by application of different methodologies such as analytical  
 solutions [29], the Boundary Element Method (BEM) [30] or the Finite Element  
 Method (FEM) [31]. The limitation of this approach is that it describes prop-  
 agation of the debond, not its initiation. Finite fracture mechanics [32] is one  
 way how to address the initiation problem. Different works have followed the  
 50 LEFM approach and studied models of one or two fibers in an effectively infinite  
 matrix [33, 34, 35, 36, 37] and of an hexagonal cluster of fibers in an effectively  
 infinite homogenized UD composite [38, 31]. The problem of debond growth  
 along the fiber-matrix interface in a cross-ply laminate has been only addressed  
 very recently in [39, 40], where authors embed a single partially debonded fiber  
 55 in an effectively infinite homogenized  $90^\circ$  ply bounded by homogenized  $0^\circ$  lay-  
 ers. Thus, the effect of debond-debond interaction and of the relative proximity  
 of a  $0^\circ/90^\circ$  interface on the debond's ERR in cross-ply laminates is yet to be  
 addressed. The present work is devoted to this problem. Models of Repeating  
 Unit Cells (RUCs) are developed to represent laminates with different degrees  
 60 of damage (here only in the form of debonds). The number of fully bonded  
 fibers across the thickness of the  $90^\circ$  ply is varied in order to investigate the  
 effect of the proximity of the  $0^\circ/90^\circ$  interface. The thickness of the bounding  $0^\circ$   
 layers is also used as a parameter of the study. The stress and strain fields are  
 solved with the Finite Element Method in Abaqus [41] and the debond (crack)  
 65 is characterized by its Mode I and Mode II ERR, calculated with the VCCT  
 and the J-integral method.

## 2. RVE models & FE discretization

### 2.1. Introduction & Nomenclature

In the present work, we investigate debond development under in-plane  
70 transverse tension in  $[0_{m \cdot 2l}^{\circ}, 90_l^{\circ}]_S$  laminates, where  $2l$  is the thickness of the  
central  $90^{\circ}$  layer expressed in terms of the number  $l$  of plies constituting it and  
 $m \cdot 2l$  represents the thickness of the  $0^{\circ}$  layer as a multiple of the  $90^{\circ}$  layer  
thickness. The interaction between debonds in the presence of an interface with  
a stiff layer is studied with the use of different Repeating Unit Cells (RUCs)  
75 (see Figures 1 and 2 in Sec. 2.2), in which only the central fiber is partially  
debonded. Repetition of the composite RUC can occur only along the in-plane  
transverse direction, thus representing a cross-ply laminate with a thin or even  
ultra-thin  $90^{\circ}$  ply in the middle.

The thickness of the  $90^{\circ}$  ply depends on the number of fibers present across the  
80 thickness (the vertical or  $z$  direction in Figures 1 and 2) and the value of the  
fiber volume fraction  $V_f$ . On the other hand, the thickness of the  $0^{\circ}$  layers can  
be assigned freely as a multiple of the  $90^{\circ}$  ply thickness, i.e.  $t_{0^{\circ}} = m \cdot t_{90^{\circ}}$  where  
 $m$  is an arbitrary integer. Thus, the thickness ratio  $i$  represents one additional  
parameter for the investigation. In the RUCs proposed, we consider the  $90^{\circ}$   
85 ply with debonds as a series of stacked damaged and undamaged fiber rows,  
each row with only one fiber in the thickness direction. All the RUCs present  
regular microstructures with fibers placed according to a square-packing con-  
figuration and consequently they are Representative Volume Elements (RVE)  
of cross-ply laminates with a certain distribution of debonds in the middle  $90^{\circ}$   
90 layer. In the following, let us consider in-plane coordinates  $x$  and  $y$ , where  $x$   
is in the transverse direction of the cross-ply laminate under consideration. In  
the presence of a load in the  $x$ -direction, the strain in the  $y$ -direction is small,  
due to the very small Poisson's ratio of the laminate. Furthermore, debonds are  
considered to be significantly longer in the fiber direction than in the arc direc-  
95 tion [42]. Therefore we use 2D models under the assumption of plane strain,  
defined in the  $x - z$  section of the composite. The study presented in this paper

thus applies to long debonds and its focus is on understanding the mechanisms of growth along their arc direction. The laminates are assumed to be subject to transverse tensile strain, which is applied in the form of a constant displacement in the  $x$ -direction along both vertical boundaries of the RUC as shown in Figure 3.

In summary, the models are differentiated by: first, the spacing between debonds along the horizontal direction in the  $90^\circ$  layer, which corresponds to the number  $n$  of fibers in the RUC's horizontal direction; second, the thickness of the middle  $90^\circ$  ply measured in terms of the number  $k$  of fiber rows; third, the factor  $m$  which provides the thickness of the  $0^\circ$  layers as an integer multiple of the  $90^\circ$  ply thickness. It thus seems natural to introduce a common notation in the presented results as  $n \times k - m \cdot t_{90^\circ}$ . An additional model is considered to study the effect of equivalent boundary conditions. This final model is constituted by only one partially debonded fiber. The application of coupling of horizontal displacements in the form of a constant applied displacement along the right and left sides allows for repetition along the horizontal direction. The presence of coupling of vertical displacements and a linear distribution of horizontal displacements on the bottom and top surfaces models the presence of the interface between the  $90^\circ$  layer and the stiff  $0^\circ$  one. This model is referred to as  $1 \times 1 - H + V$  given that: it has respectively 1 fiber in the horizontal and in the vertical direction; on the top and bottom surfaces, both horizontal (H) and vertical (V) displacements are assigned. Furthermore, two single fiber models similar to  $1 \times 1 - H + V$  are considered in the present work for comparison: the  $1 \times 1 - free$  and  $1 \times 1 - coupling$ . In the first, the upper surface is left free; in the second, vertical displacement coupling is applied to the upper boundary. Further details about these models and the corresponding laminate RVE can be found in [43].

## 2.2. Description of modelled Representative Volume Elements (RVEs)

The first family of Representative Volume Elements (RVEs) is represented in Figure 1. It represents a set of  $[0_{m \cdot 2l}^\circ, 90_l^\circ]_S$  cross-ply laminates with an

ultra-thin  $90^\circ$  layer, constituted by a single row of fibers across the thickness. Debonds appear at regular intervals measured in terms of number  $n - 1$  of fully bonded fibers present between them, which in turn correspond to the number of fibers along the horizontal direction of the RVE as highlighted in Fig. 1. They are thus the  $n \times 1 - m \cdot t_{90^\circ}$  models, where  $m = 1, 10$  and  $n$  is an integer  $\geq 1$  ( $n = 1$  corresponds to the case of a debond appearing on all the fibers in the central  $90^\circ$  layer). These models are geometrically extreme, but allow to focus on the interaction between debonds and the inter-ply  $0^\circ/90^\circ$  interface. Furthermore, the *spread tow* technology is today capable of producing cross-ply laminates with the central  $90^\circ$  layer thickness only 4–5 times the fiber diameter, as shown for example in [9], which may in future give practical relevance even to such extreme case.

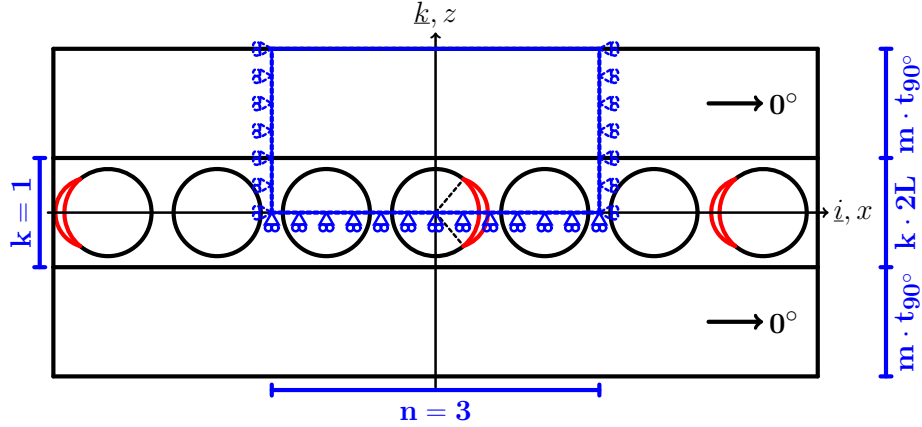


Figure 1: Models of  $[0_{m \cdot 2L}^\circ, 90_l^\circ]_S$  laminates with an ultra-thin  $90^\circ$  layer, where the  $90^\circ$  ply is made up by a single “row” of fibers. Debonds are repeating at different distances, measured in terms of the number  $n - 1$  of fully bonded fibers appearing between two consecutive debonds.  $2L$  is the thickness of one-fiber row.

The second set of models considers instead cross-ply laminates with a central  $90^\circ$  ply of variable thickness, measured in terms of number  $k$  of fiber rows appearing in the vertical direction in Figure 2. Once again, debonds appear in the central row only at regular intervals measured in terms of number  $n - 1$  of fully bonded fibers present between them, which in turn correspond to the

number of fibers along the horizontal direction of the RUC as highlighted in  
 145 Fig. 2. These models are thus the  $n \times k - m \cdot t_{90^\circ}$  models, where  $i = 1, 10$ ,  $k > 1$   
 and  $n$  is an integer  $\geq 1$  ( $n = 1$  corresponds to the case of a debond appearing  
 on all fibers of the central fiber row in the  $90^\circ$  layer).

By increasing the number  $n$  of fibers in the horizontal direction in the RUC,  
 decreasing levels of damage (debonds spaced further apart and the interaction  
 150 between debonds becomes less important) are considered to be present in the  
 laminate. By increasing the number  $k$  of fiber rows, the thickness of the  $90^\circ$   
 layer is increased and the effect of the relative proximity of the inter-ply  $0^\circ/90^\circ$   
 interface can thus be studied. Finally, by increasing the factor  $m$ , the thickness  
 of the  $0^\circ$  layers is increased for a given thickness of the  $90^\circ$ , which allows the  
 155 investigation of the  $0^\circ$  ply-block effect [44].

### 2.3. Finite Element (FE) discretization

The RUCs are discretized and solved with the Finite Element Method (FEM)  
 using the commercial FEM package Abaqus [41]. The length  $l$  and height  $h$  of  
 the model are determined by the number of fibers  $n$  in the horizontal direction,  
 160 the number of fiber rows  $k$  across the thickness and the thickness ratio  $i$  (see  
 Sec. 2.2) according to Eq. 1:

$$l = 2nL \quad h = (1 + 2i)kL. \quad (1)$$

In Eq. 1,  $2L$  is the length of a one-fiber unit (see Fig. 3), which in turn is as  
 a function of the fiber volume fraction  $V_f$  and the fiber radius according to

$$L = \frac{R_f}{2} \sqrt{\frac{\pi}{V_f}}. \quad (2)$$

Each fiber in the model has the same radius  $R_f$ , equal to  $1 \mu m$ . This specific  
 165 value has no physical meaning per se and it has been selected for simplicity. It  
 is useful to observe that, in a linear elastic solution as the one described in the  
 present article, the ERR is proportional to the geometrical dimensions of the  
 model and thus re-evaluation of the ERR for fibers of any size requires just

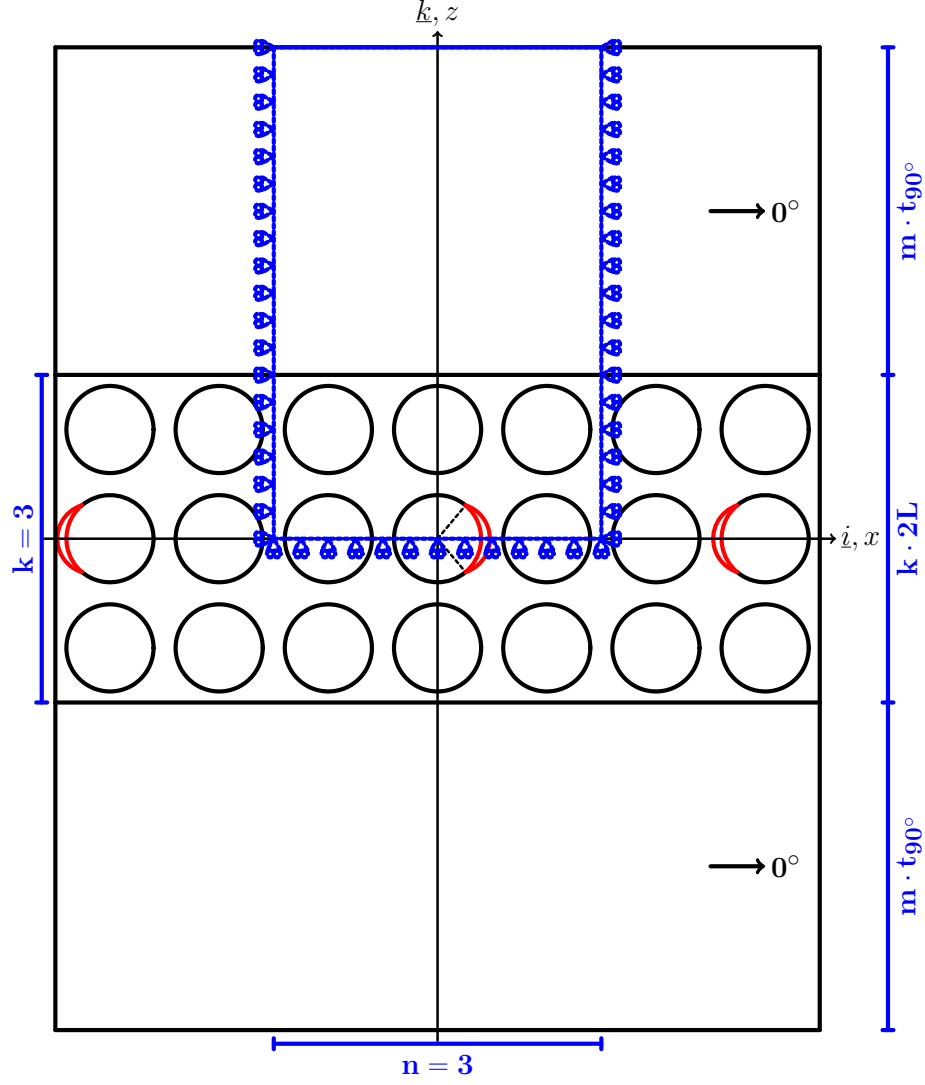


Figure 2: Models of  $[0_{m \cdot 2L}^{\circ}, 90_l^{\circ}]_S$  laminates with a  $90^{\circ}$  layer of variable thickness, determined by the number  $k$  of “rows” of fibers along the vertical direction. Debonds are repeating at different distances along the horizontal direction, measured in terms of the number  $n - 1$  of fully bonded fibers appearing between two consecutive debonds.  $2L$  is the thickness of one-fiber row.

a multiplication. Furthermore, the local and global  $V_f$  are everywhere equal thanks to the relationships in Eqs. 1 and 2.



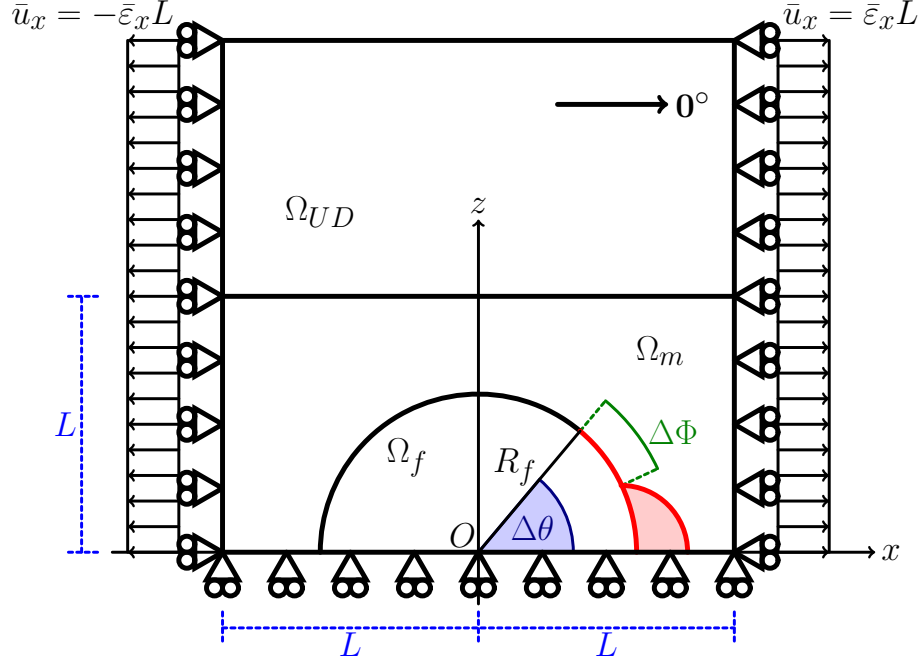


Figure 3: Schematic of the model with its main parameters.

The debond appears symmetrically with respect to the  $x$  axis (see Fig. 3) and we characterize it with the angular size  $\Delta\theta$  (the full debond size is thus  $2\Delta\theta$ ). In the case of large debond sizes ( $\geq 60^\circ - 80^\circ$ ), a region of size  $\Delta\Phi$  to be determined by the solution itself appears at the crack tip. In this region, called the *contact zone*, the crack faces are in contact and slide on each other. Due to existence of the contact zone, frictionless contact is considered between the two crack faces to avoid interpenetration and allow free sliding. Symmetry with respect to the  $x$  axis is applied on the lower boundary. The upper boundary is free, except for the model  $1 \times 1 - H + V$  which requires on the upper side kinematic coupling of vertical displacements and applied linearly distributed horizontal displacements. Kinematic coupling on the  $x$ -displacement is applied along the left and right boundaries of the model in the form of a constant  $x$ -displacement  $\pm \bar{\epsilon}_x l$ , corresponding to transverse strain  $\bar{\epsilon}_x$  equal to 1%.

The FEM model is discretized using second order, 2D, plane strain triangu-

Table 1: Summary of mechanical properties of fiber, matrix and UD layer.  $E$  stands for Young’s modulus,  $\mu$  for shear modulus and  $\nu$  for Poisson’s ratio. Indexes  $L$  and  $T$  stand respectively for *longitudinal* and *transverse*.

<b>Material</b>	$V_f$ [%]	$E_L$ [GPa]	$E_T$ [GPa]	$\mu_{LT}$ [GPa]	$\nu_{LT}$ [–]	$\nu_{TT}$ [–]
Glass fiber	-	70.0	70.0	29.2	0.2	0.2
Epoxy	-	3.5	3.5	1.25	0.4	0.4
UD	60.0	43.442	13.714	4.315	0.273	0.465

lar (CPE6) and rectangular (CPE8) elements. In the crack tip neighborhood, a refined regular mesh of quadrilateral elements with almost unitary aspect ratio is needed to ensure a correct evaluation of the ERR. The angular size  $\delta$  of an element in this refined region close to the crack tip is by design equal to  $0.05^\circ$ . The crack faces are modeled as element-based surfaces with a frictionless small-sliding contact pair interaction. The Mode I, Mode II and total Energy Release Rates (ERRs) (respectively  $G_I$ ,  $G_{II}$  and  $G_{TOT}$ ) represent the main result of the numerical analysis. They are computed using the VCCT [27] implemented in a custom Python routine and the total ERR is obtained from the J-integral [28] evaluation by means of the Abaqus built-in functionality. Glass fiber and epoxy are considered throughout this article, and it is assumed that their response always lies in the linear elastic domain. The effective UD properties are computed using Hashin’s Concentric Cylinder Assembly model [45] with the self-consistency scheme for the out-of-plane shear modulus of Christensen [46]. The properties used are listed in Table 1. The model was validated with respect to BEM results of [47, 36]; considerations about the order of accuracy can be found in [43].

### 3. Results & Discussion

#### 3.1. Effect of the proximity of the $0^\circ/90^\circ$ interface and of the thickness of the $0^\circ$ layer on debond ERR

205 We first focus our attention on the model  $1 \times 1 - m \cdot t_{90^\circ}$ , which represents a particular case of the family  $n \times 1 - m \cdot t_{90^\circ}$ . It corresponds to a cross-ply laminate in which the central  $90^\circ$  ply is constituted by only one fiber row, in which each fiber possesses a debond appearing on alternating sides. The model thus represents an extreme idealization, in the sense that: first, the central  $90^\circ$  210 layer is the thinniest that can be conceived; second, a very particular damage state is present for which every fiber is partially debonded from the surrounding matrix. The first condition allows us to investigate the direct effect of the proximity of the  $0^\circ/90^\circ$  interface on debond ERR. The second condition implies that we are analyzing the most severe damage state that can occur in the  $90^\circ$  215 ply when considering debonds as the only mechanism of damage. As pointed out in a previous work [43], the presence of fully bonded fibers close to the partially debonded one causes a magnification of the  $x$ -strain in the matrix region between the debonded fiber and the closest undamaged one. This increase in the value of the strain leads in turn to higher values of Energy Release Rate. 220 Given that we are considering a  $90^\circ$  ply with all fibers partially debonded, we are neglecting such magnification effect and focusing only on the presence of the  $0^\circ/90^\circ$  interface and on the thickness of the  $0^\circ$  layer, by considering the ratio  $m = \frac{t_{0^\circ}}{t_{90^\circ}}$  of ply thicknesses as a free parameter. We will later analyze in Sec. 3.2 the effect of the combined presence of fully bonded fibers and the 225  $0^\circ/90^\circ$  interface.

In Figures 4 and 5 respectively the Mode I and Mode II ERR are shown for models  $1 \times 1 - m \cdot t_{90^\circ}$  with  $m = 1, 10, 50, 100$  and models  $1 \times 1 - free$ ,  $1 \times 1 - coupling$  and  $1 \times 1 - H + V$ . It is worth to remind us of the laminate RVE that correspond to these last three models: model  $1 \times 1 - free$  represents 230 a one-fiber-row UD composite with all the fibers partially debonded; model  $1 \times 1 - coupling$  corresponds to a UD laminate with an infinite number of fiber

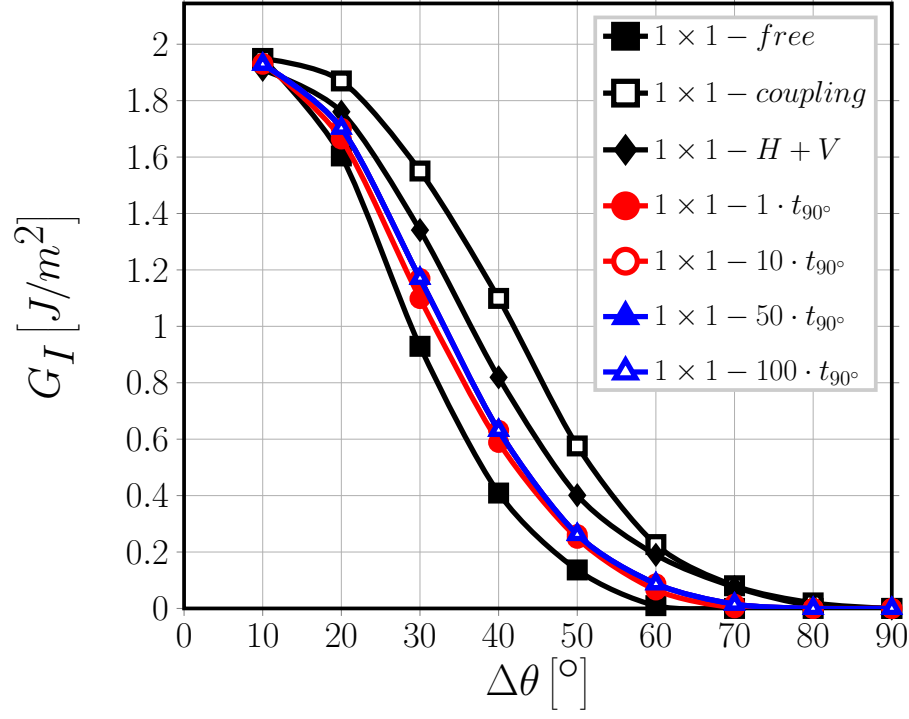


Figure 4: Effect of the proximity of the  $0^\circ/90^\circ$  interface and of the thickness of the  $0^\circ$  layer on Mode I ERR: models  $1 \times 1 - free$ ,  $1 \times 1 - coupling$ ,  $1 \times 1 - H + V$  and  $1 \times 1 - m \cdot t_{90^\circ}$ .  $V_f = 60\%$ ,  $\varepsilon_x = 1\%$ .

rows and all the fibers partially debonded; model  $1 \times 1 - H + V$  represents a cross-ply laminate with one-fiber-row central  $90^\circ$  ply and the  $0^\circ$  ply replaced by boundary conditions at the interface not allowing interface bending and with an applied uniform strain not affected by fibers and debonds in the  $90^\circ$  ply. Observing Figure 4, it is possible to notice that the values of  $G_I$  for the  $1 \times 1 - free$  and the  $1 \times 1 - coupling$  model represent respectively a lower and an upper bound for all the other RVEs. The  $1 \times 1 - H + V$  model is as well an upper bound for the  $1 \times 1 - m \cdot t_{90^\circ}$  RVEs; however its values of  $G_I$  are lower than those of the  $1 \times 1 - coupling$  model due to the applied uniform  $x$ -strain at the interface, which prevents the crack to open as much as in the  $1 \times 1 - coupling$  case. The same observation holds for the size of the debond at contact zone

onset, i.e. when  $G_I = 0$ : the lower bound is provided by the  $1 \times 1 - free$  model ( $\Delta\theta \sim 60^\circ$ ), while the contact zone onset for models  $1 \times 1 - coupling$  and  $1 \times 1 - H + V$  represents the upper bound ( $\sim 80^\circ$ ). All  $1 \times 1 - m \cdot t_{90^\circ}$  RVEs lie in between these two bounds for any thickness of the  $0^\circ$  ply, with contact zone onset occurring at a debond size of  $\sim 70^\circ$ .

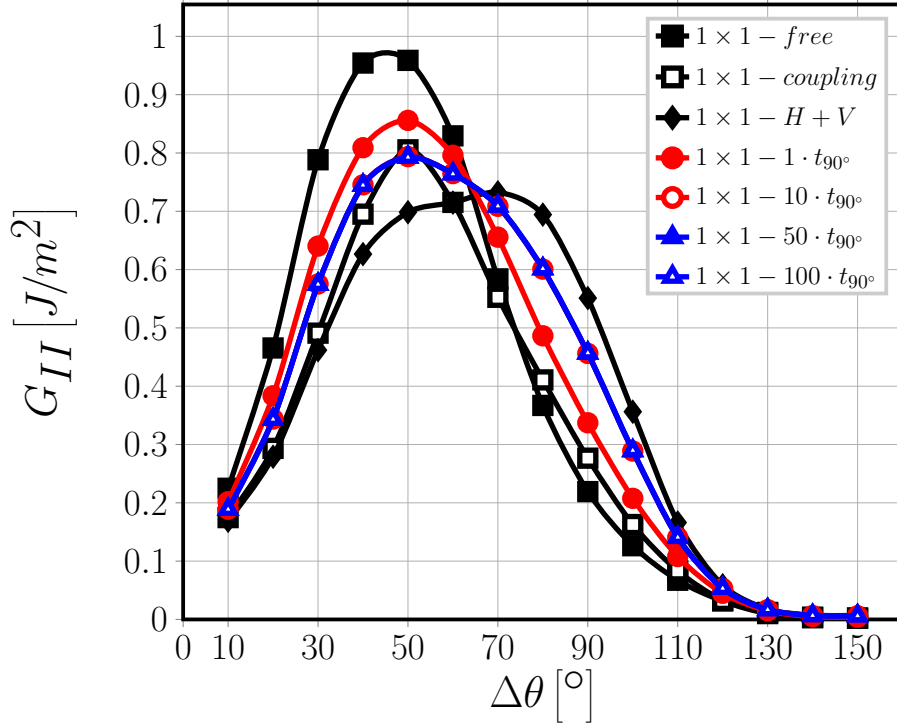


Figure 5: Effect of the proximity of the  $0^\circ/90^\circ$  interface and of the thickness of the  $0^\circ$  layer on Mode II ERR: models  $1 \times 1 - free$ ,  $1 \times 1 - coupling$ ,  $1 \times 1 - H + V$  and  $1 \times 1 - m \cdot t_{90^\circ}$ .  $V_f = 60\%$ ,  $\varepsilon_x = 1\%$ .

For Mode II (see Fig. 5), the ERR for the cases with a  $0^\circ$  layer of finite thickness always lies between the values provided by the  $1 \times 1 - free$  and  $1 \times 1 - H + V$  model: for open debonds ( $\Delta\theta < 60^\circ - 70^\circ$ ), when  $G_I \neq 0$  and there is no contact zone,  $1 \times 1 - free$  provides the upper bound while  $1 \times 1 - H + V$  the lower bound; for close debonds ( $\Delta\theta > 60^\circ - 70^\circ$ ), when  $G_I = 0$  and a contact zone is present, the situation is reversed. An effect of the thickness of the  $0^\circ$  layer

on Mode II ERR can be noticed in Fig. 5 when the ratio  $m = \frac{t_{0^\circ}}{t_{90^\circ}}$  is increased  
 255 from 1 to 10. The change between the two follows the same pattern described  
 previously: when the thickness of the  $0^\circ$  ply is increased, Mode II decreases for  
 open debonds and increases for closed debonds, in line with the bound switch.  
 These results help to shed light on the effect of the  $0^\circ/90^\circ$  interface on debond  
 ERR. The presence of the stiff homogenized  $0^\circ$  layer causes the matrix placed  
 260 relatively far from the fiber (close to the interface) to contract much less than  
 it would do in the presence of a free surface due to its relatively high Poisson's  
 ratio. Furthermore, the presence of the  $0^\circ/90^\circ$  interface induces a more  
 homogeneous  $x$ -displacement field all over the matrix domain. This causes a  
 concurrent increase of  $G_I$  and decrease of  $G_{II}$  for small debonds, where the  
 265 crack opening displacement component at the crack tip (responsible for Mode  
 I) is mostly due to the global  $x$ -displacement field (which increases in the presence  
 of the  $0^\circ/90^\circ$  interface) while the crack sliding displacement component at  
 the crack tip (responsible for Mode II) is for small debonds linked to the global  
 vertical displacement field due to Poisson's effect (which is lower in the presence  
 270 of a  $0^\circ$  layer instead of a free surface thanks to the stiffness of the former).  
 This causes also the delay in the onset of the contact zone. For large debonds  
 instead, after the onset of the contact zone, the situation reverses: the magnitude  
 increase of the global  $x$ -displacement field leads to an increase in the crack  
 sliding displacement component at the crack tip and thus in Mode II ERR. By  
 275 comparing the results for Mode II of models  $1 \times 1 - free$ ,  $1 \times 1 - H + V$  and  
 $1 \times 1 - m \cdot t_{90^\circ}$  with  $m = 1, 10, 50, 100$  (Fig. 5), it can be argued that the effect  
 of the  $0^\circ$  ply thickness is related to its local bending stiffness. In the presence  
 a free surface, the matrix in the  $90^\circ$  ply contracts significantly more than the  
 fibers due to the mismatch in Poisson's ratios, thus leading to higher  $y$ -strains  
 280 in the inter-fibers regions than above the fibers. This in turn results in a very  
 curved surface, roughly following the fibers' curvature. In the presence of a  $0^\circ$   
 layer, such deformation is prevented by its bending stiffness. A relatively thin  
 $0^\circ$  layer ( $\frac{t_{0^\circ}}{t_{90^\circ}} = 1$ ) possesses a lower bending stiffness and thus matrix deformation  
 is able to bend the interface, which translates into a  $G_{II}$  profile closer

285 to the  $1 \times 1 - free$  model. For thicker  $0^\circ$  layers, the increased bending stiffness prevents the curvature of the interface and Mode II ERR becomes closer to the  $1 \times 1 - H + V$  model, in which the interface is forced to remain straight by the applied boundary conditions.

### 3.2. Effect of the proximity of the $0^\circ/90^\circ$ interface on debond-debond interaction 290 in a single fiber row $90^\circ$ ply

We turn now our attention to the model  $n \times 1 - 1 \cdot t_{90^\circ}$ , which corresponds to a cross-ply laminate in which the central  $90^\circ$  ply is constituted by only one fiber row where multiple partially debonded fibers are present, located at a distance of  $n - 1$  fully bonded fibers from each other, and debonds appear on alternating  
295 sides of consecutive damaged fibers (see Figure 1). This class of models allows to study the effect of the presence of the  $0^\circ$  layer on debond-debond interaction and, particularly, crack shielding [48, 43].

In the presence of a free surface, both Mode I and Mode II ERR increase rapidly when the number of fully bonded fibers placed between two consec-  
300 utive partially debonded one is increased ( $n \times 1 - free$  models in Figures 6 and 7). The presence of fully bonded fibers causes an increase in the local  $x$ -strain in the debond neighborhood, which leads to greater crack opening and sliding displacements and thus higher ERR (strain magnification [43]). The same mechanism can be described from the opposite point of view: increasing  
305 the number of debonds present in the  $90^\circ$  ply reduces the stress concentration in the inter-fibers regions and thus results in lower values of the ERR (crack shielding [48, 43]). From Figures 6 and 7 it seems apparent that the strain magnification effect is present in cross-ply laminates as well, albeit strongly reduced by the presence of the  $0^\circ/90^\circ$  interface. This effect is less evident when  
310 debonds are close to each other ( $1 \times 1 - 1 \cdot t_{90^\circ}$  and  $3 \times 1 - 1 \cdot t_{90^\circ}$ ), i.e. in the case of more severe damage states.

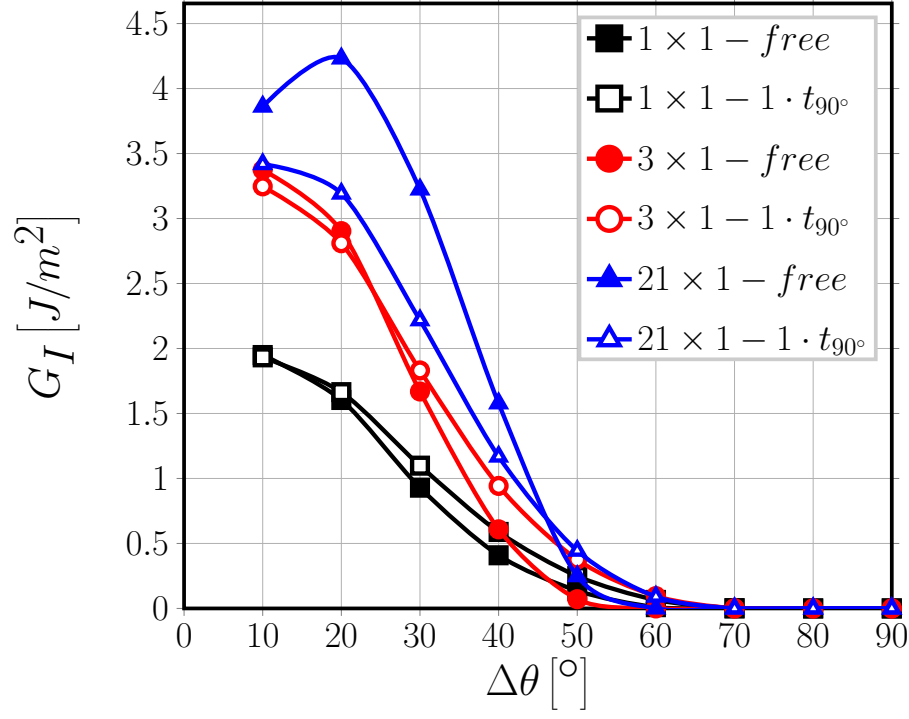


Figure 6: Effect of the presence of the  $0^\circ$  layer on debond-debond interaction for Mode I ERR: models  $n \times 1 - free$  and  $n \times 1 - 1 \cdot t_{90^\circ}$ .  $V_f = 60\%$ ,  $\varepsilon_x = 1\%$ .

### 3.3. Effect of the presence of fiber rows with no damage on the debond- $0^\circ/90^\circ$ interface interaction

After having investigated the effect of the proximity of the  $0^\circ/90^\circ$  interface and of the thickness of the  $0^\circ$  layer on debond ERR and on debond-debond interaction, we address in this section the effect of the presence of fiber rows with only fully bonded fibers inside on the interaction between debonds and the  $0^\circ/90^\circ$  interface. In other words, we are separating the debond from the interface by inserting rows of fully bonded fibers in between, thus increasing the distance to the interface. To this end, we study the models  $1 \times k - 1 \cdot t_{90^\circ}$ , which represent a cross-ply laminate with the central  $90^\circ$  ply made of  $k$  fiber rows and where all the fibers in the central row are partially debonded. The absence of fully bonded fibers in the central row prevents the occurrence of



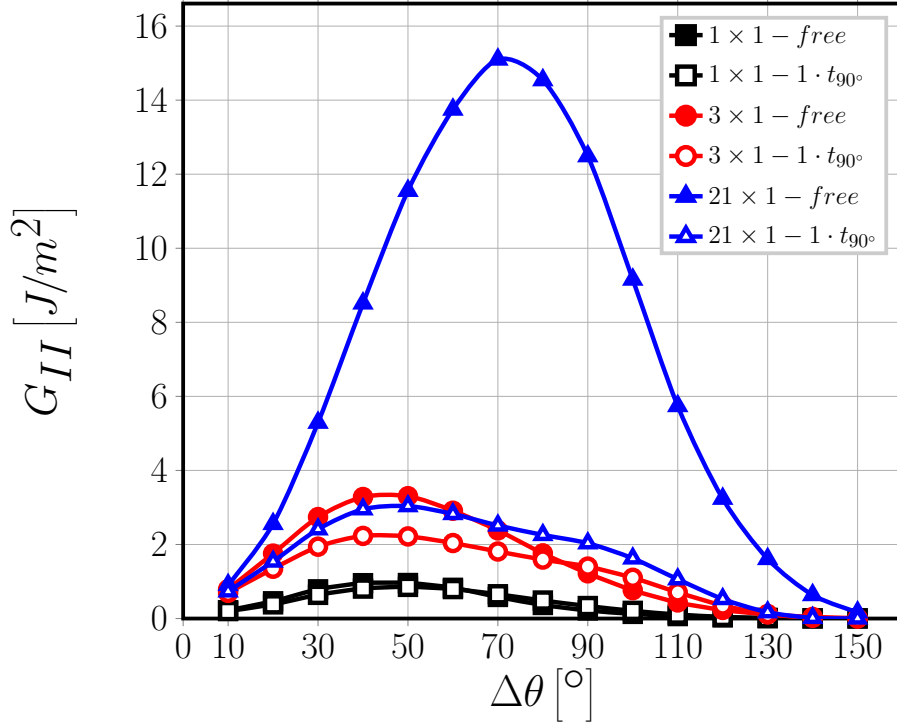


Figure 7: Effect of the presence of the  $0^\circ$  layer on debond-debond interaction for Mode II ERR: models  $n \times 1 - free$  and  $n \times 1 - 1 \cdot t_{90^\circ}$ .  $V_f = 60\%$ ,  $\varepsilon_x = 1\%$ .

strain magnification or crack shielding (see Sec. 3.2), thus allowing to focus on  
the effect of the distance of the  $0^\circ/90^\circ$  interface (measured in terms of rows of  
fully bonded fibers).

Figures 8 and 9 thus show the effect on ERR of the presence of the  $0^\circ$  ply in  
the case of non-interacting debonds (no strain magnification or crack shielding).  
If the distance between the  $0^\circ/90^\circ$  interface and the debond is at least one fully  
bonded fiber, the presence of the  $0^\circ$  ply does not influence debond ERR and  
no measurable difference can be observed between models  $1 \times k - free$  and  
 $1 \times k - 1 \cdot t_{90^\circ}$  for  $k \geq 1$ .

However, the situation changes when fully bonded fibers are present between  
consecutive partially debonded fibers, as shown in Figures 10 and 11. For Mode  
I ERR (Fig. 10), the presence of one row of fully bonded fibers already prevents

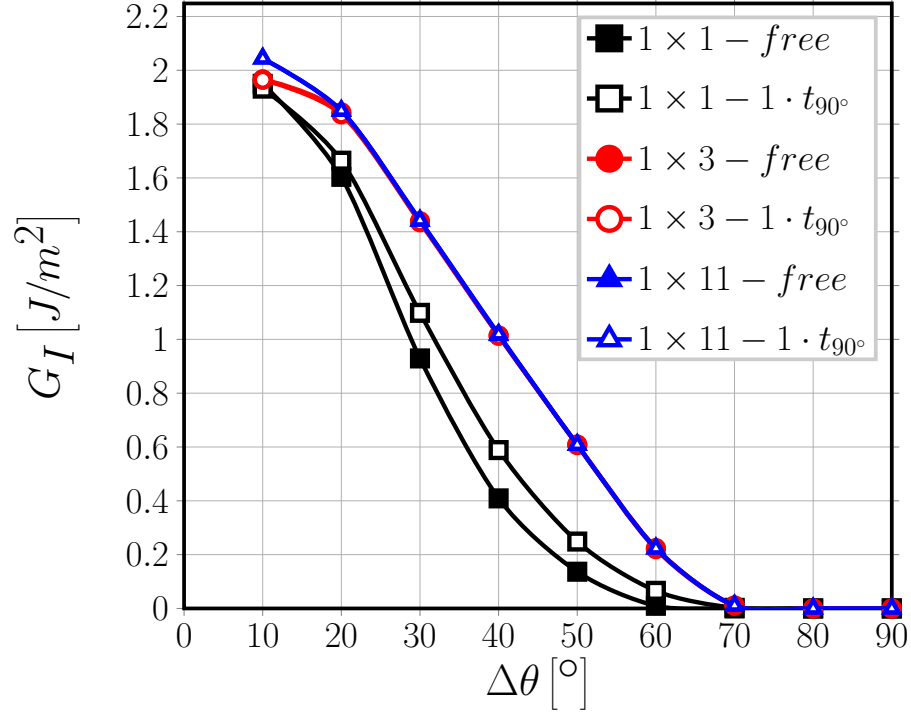


Figure 8: Effect of the presence of undamaged fiber rows in the  $90^\circ$  layer on debond- $0^\circ/90^\circ$  interface interaction for Mode I ERR: models  $1 \times k - free$  and  $1 \times k - 1 \cdot t_{90^\circ}$ .  $V_f = 60\%$ ,  $\varepsilon_x = 1\%$ .

the  $0^\circ$  ply from having any measurable effect on debond ERR: no difference can be seen between results for models  $n \times k - free$  and models  $n \times k - 1 \cdot t_{90^\circ}$ . Thus, the effect of strain magnification on  $G_I$  (Sec. 3.2) in cross-ply laminates follows the same pattern as in UD composites. A more noticeable effect of the presence of the  $0^\circ$  ply can be observed for Mode II (Fig. 11): it causes a reduction in the ERR, particularly when debonds are far apart (models  $21 \times 3 - free$  and  $21 \times 3 - 1 \cdot t_{90^\circ}$ ), thus mitigating the strain magnification effect for Mode II.

In [39, 40], the authors investigate the existence of a ply-thickness effect on the fiber-matrix interface crack using two models with respectively an isolated and two neighboring debonded fibers embedded in a homogenized  $90^\circ$  ply bounded by homogenized  $0^\circ$  layers. They select the thickness of the  $0^\circ$  layer as

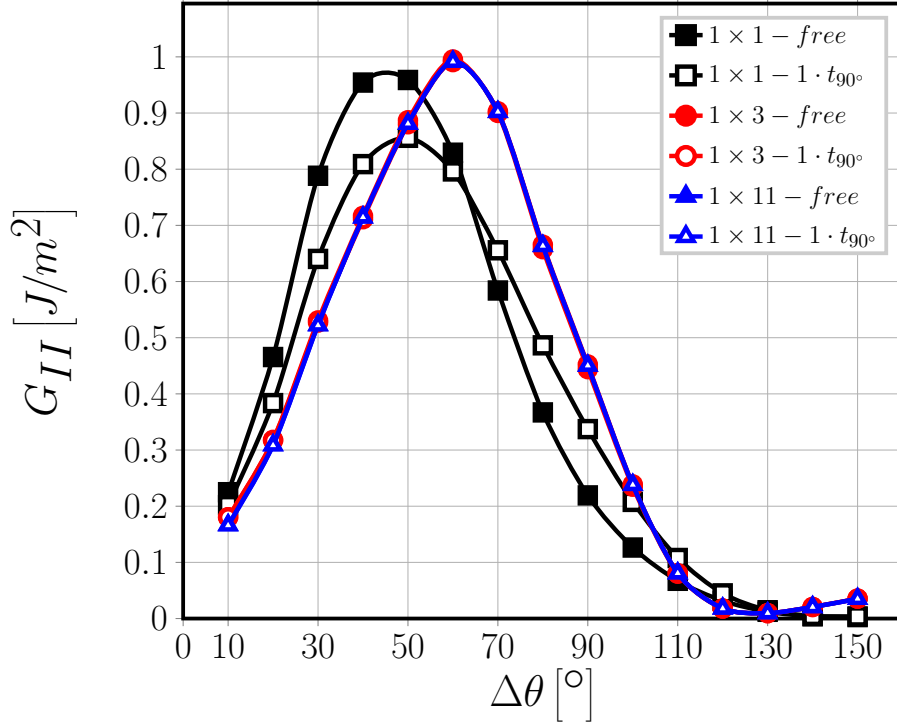


Figure 9: Effect of the presence of undamaged fiber rows in the  $90^\circ$  layer on debond- $0^\circ/90^\circ$  interface interaction for Mode II ERR: models  $1 \times k - free$  and  $1 \times k - 1 \cdot t_{90^\circ}$ .  $V_f = 60\%$ ,  $\varepsilon_x = 1\%$ .

reference and model a  $[0_p^\circ, 90_{r.p}^\circ]_S$  laminate. The thickness of the  $90^\circ$  ply, measured relatively to the thickness of the  $0^\circ$  layer through the factor  $r$ , represents the main parameter of the study, varying from  $r = 3$  (thick  $90^\circ$  ply,  $> 100$  fiber diameters) to  $r = 0.1$  (ultra-thin  $90^\circ$  ply,  $\sim 4 - 5$  fiber diameters). No measurable ply-thickness effect is observed. The results presented in this article confirm their observation and provide a micromechanical explanation (see Sec. 3.1). We have also shown that extremely thin  $90^\circ$  plies ( $1 - 5$  fiber diameters thick) are on the other hand subject to the strain magnification effect when fully bonded fibers appear between consecutive aligned debonds. The only effect of the  $0^\circ$  ply is to reduce the magnification of ERR, which nonetheless takes place. However, this mechanism is not peculiar only of cross-ply laminates, but it can be ob-

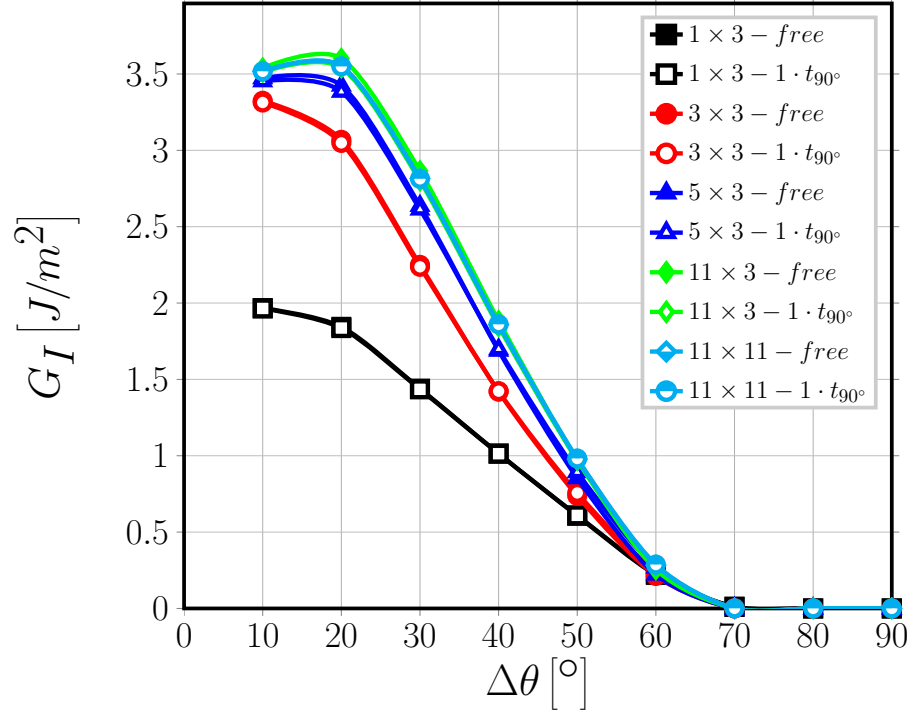


Figure 10: Effect of the presence of undamaged fiber rows in the  $90^\circ$  layer on debond- $0^\circ/90^\circ$  interface interaction for Mode I ERR: models  $n \times k - free$  and  $n \times k - 1 \cdot t_{90^\circ}$ .  $V_f = 60\%$ ,  $\varepsilon_x = 1\%$ .

served in UD composites as well [43]. The results proposed in this paper could provide a possible mechanical description of the observations presented in [9].

360 The authors conducted *in-situ* observations of edge micro-cracks with an optical microscope on  $[0_2^\circ, 90_n^\circ, 0_2^\circ]$  carbon fiber-epoxy laminates with  $n = 1, 2, 4$ , corresponding to a  $90^\circ$  ply thickness of respectively  $40 [\mu m]$  ( $\sim 6 - 8$  fiber diameters),  $80 [\mu m]$  ( $\sim 12 - 16$  fiber diameters) and  $160 [\mu m]$  ( $\sim 24 - 32$  fiber diameters). For  $n = 1$ , i.e. the case of a very thin  $90^\circ$  ply, isolated debonds appear at a  
365 lower value of the applied strain than in thicker plies (at  $0.4\%$  vs  $0.7\%$ ) while coalescence of debonds is suppressed and no transverse crack can be observed even at a strain of  $1.5\%$ . It has been shown in this work that in thin  $90^\circ$  plies, i.e. with  $< 10$  fibers across the thickness, a relevant strain magnification effect

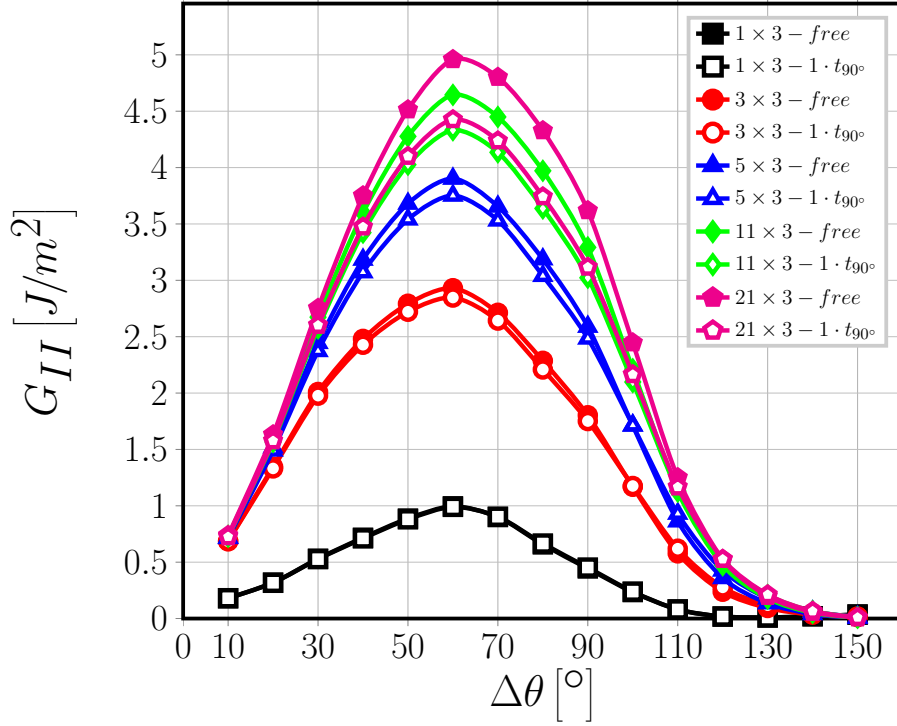


Figure 11: Effect of the presence of undamaged fiber rows in the  $90^\circ$  layer on debond- $0^\circ/90^\circ$  interface interaction for Mode II ERR: models  $n \times k - free$  and  $n \times k - 1 \cdot t_{90^\circ}$ .  $V_f = 60\%$ ,  $\varepsilon_x = 1\%$ .

can be observed when debonds are far from each other and separated by fully bonded, which causes an increase in ERR. This in turn makes the growth of debonds more likely to occur at lower levels of strain than in thick plies (the ERR is proportional to  $\varepsilon^2$  in LEFM), which would explain the observations reported in [9].

#### 4. Conclusions

Different models of Repeating Unit Cell, representing different cross-ply laminates, have been studied in order to study the effect of the presence of the  $0^\circ$  layer and of its thickness on debond Energy Release Rate and on crack shielding. It has been found that the presence of the  $0^\circ$  ply does not significantly

alter the trends in ERR observed for the same  $90^\circ$  ply thickness and damage  
 380 configuration in UD models [43], albeit reducing in general the estimated values  
 of  $G_I$  and  $G_{II}$ . Furthermore, it has been observed that the influence of the  $0^\circ$   
 layer is strongly mitigated by the presence of rows of undamaged fibers between  
 the debond and the  $0^\circ/90^\circ$  interface. Already the presence of only 1 row of  
 fully bonded fibers between respectively the upper and lower  $0^\circ$  layer and the  
 385 central fiber row with partially debonded fibers causes the Mode I and Mode II  
 ERR to adhere closely to the UD results. The observations presented provide  
 an important insight: it appears that the behavior of the fiber/matrix interface  
 crack is affected strongly only by very close perturbation of the elastic fields.  
*Thin* and *ultra-thin* plies present a peculiar behavior in terms of debond growth  
 390 because their reduced thickness brings the  $0^\circ/90^\circ$  interface close enough for the  
 debonds to feel the perturbation in the elastic fields. Otherwise, it seems that  
 no difference can be found in the mechanism of debond growth between a UD  
 composite and a cross-ply laminate.

## Acknowledgements

395 Luca Di Stasio gratefully acknowledges the support of the European School  
 of Materials (EUSMAT) through the DocMASE Doctoral Programme and the  
 European Commission through the Erasmus Mundus Programme.

## References

- [1] K. Kawabe, New spreading technology for carbon fiber tow and its ap-  
 400 plication to composite materials, *Sen'i Gakkaishi* 64 (8) (2008) 262–267.  
 doi:10.2115/fiber.64.p\_262.
- [2] K. Kawabe, H. Sasayama, S. Tomoda, New carbon fiber tow-spread tech-  
 nology and applications to advanced composite materials, *SAMPE Journal*  
 45 (2) (2008) 6–17.

- 405 [3] H. Sasayama, K. Kawabe, S. Tomoda, I. Ohsawa, K. Kageyama, N. Ogata, Effect of lamina thickness on first ply failure in multidirectionally laminated composites, in: Proceedings of the 8<sup>th</sup> Japan SAMPE Symposium, SAMPE, 2003.
- [4] K. Yamaguchi, H. Hahn, The improved ply cracking resistance of thin-ply laminates, in: Proceedings of the 15<sup>th</sup> International Conference on  
410 Composite Materials (ICCM-15), SAMPE, 2005.
- [5] S. Tsai, S. Sihm, R. Kim, Thin ply composites, in: Proceedings of 46<sup>th</sup> AIAA/ASME/AHS/ASC Structures, Structural Dynamics & Materials Conference, 2005.
- 415 [6] S. Sihm, R. Kim, K. Kawabe, S. Tsai, Experimental studies of thin-ply laminated composites, Composites Science and Technology 67 (6) (2007) 996–1008. doi:10.1016/j.compscitech.2006.06.008.
- [7] T. Yokozeki, Y. Aoki, T. Ogasawara, Experimental characterization of strength and damage resistance properties of thin-ply carbon  
420 fiber/toughened epoxy laminates, Composite Structures 82 (3) (2008) 382–389. doi:10.1016/j.compstruct.2007.01.015.
- [8] T. Yokozeki, A. Kuroda, A. Yoshimura, T. Ogasawara, T. Aoki, Damage characterization in thin-ply composite laminates under out-of-plane transverse loadings, Composite Structures 93 (1) (2010) 49–57. doi:  
425 10.1016/j.compstruct.2010.06.016.
- [9] H. Saito, H. Takeuchi, I. Kimpara, Experimental evaluation of the damage growth restraining in 90 layer of thin-ply cfrp cross-ply laminates, Advanced Composite Materials 21 (1) (2012) 57–66. doi:10.1163/156855112X629522.
- 430 [10] A. Arteiro, G. Catalanotti, J. Xavier, P. Camanho, Notched response of non-crimp fabric thin-ply laminates, Composites Science and Technology 79 (2013) 97–114. doi:10.1016/j.compscitech.2013.02.001.

- [11] A. Arteiro, G. Catalanotti, J. Xavier, P. Camanho, Large damage capability of non-crimp fabric thin-ply laminates, *Composites Part A: Applied Science and Manufacturing* 63 (2014) 110–122. doi:10.1016/j.compositesa.2014.04.002.
- [12] R. Amacher, J. Cugnoni, J. Botsis, L. Sorensen, W. Smith, C. Dransfeld, Thin ply composites: Experimental characterization and modeling of size-effects, *Composites Science and Technology* 101 (2014) 121–132. doi:10.1016/j.compscitech.2014.06.027.
- [13] G. Guillaumet, A. Turon, J. Costa, J. Renart, P. Linde, J. Mayugo, Damage occurrence at edges of non-crimp-fabric thin-ply laminates under off-axis uniaxial loading, *Composites Science and Technology* 98 (2014) 44–50. doi:10.1016/j.compscitech.2014.04.014.
- [14] C. Huang, S. Ju, M. He, Q. Zheng, Y. He, J. Xiao, J. Zhang, D. Jiang, Identification of failure modes of composite thin-ply laminates containing circular hole under tension by acoustic emission signals, *Composite Structures* 206 (2018) 70–79. doi:10.1016/j.compstruct.2018.08.019.
- [15] J. Cugnoni, R. Amacher, S. Kohler, J. Brunner, E. Kramer, C. Dransfeld, W. Smith, K. Scobbie, L. Sorensen, J. Botsis, Towards aerospace grade thin-ply composites: Effect of ply thickness, fibre, matrix and interlayer toughening on strength and damage tolerance, *Composites Science and Technology* 168 (2018) 467–477. doi:10.1016/j.compscitech.2018.08.037.
- [16] J.-B. Moon, M.-G. Kim, C.-G. Kim, S. Bhowmik, Improvement of tensile properties of CFRP composites under LEO space environment by applying MWNTs and thin-ply, *Composites Part A: Applied Science and Manufacturing* 42 (6) (2011) 694–701. doi:10.1016/j.compositesa.2011.02.011.
- [17] Y. H. N. Kim, S. Ko, W.-S. Lay, J. Tian, P. Chang, S. U. Thielk, H.-J. Bang, J. Yang, Effects of shallow biangle, thin-ply laminates on structural



performance of composite wings, *AIAA Journal* 55 (6) (2017) 2086–2092.  
doi:10.2514/1.j055465.

- [18] A. Kopp, S. Stappert, D. Mattsson, K. Olofsson, E. Marklund, G. Kurth,  
E. Mooij, E. Roorda, The aurora space launcher concept, *CEAS Space*  
465 *Journal* 10 (2) (2017) 167–187. doi:10.1007/s12567-017-0184-2.
- [19] D. A. McCarville, J. C. Guzman, A. K. Dillon, J. R. Jackson, J. O. Birk-  
land, 3.5 Design, Manufacture and Test of Cryotank Components, Elsevier,  
2018, pp. 153–179. doi:10.1016/b978-0-12-803581-8.09958-6.
- [20] J. E. Bailey, A. Parvizi, On fibre debonding effects and the mechanism  
470 of transverse-ply failure in cross-ply laminates of glass fibre/thermoset  
composites, *Journal of Materials Science* 16 (3) (1981) 649–659. doi:  
10.1007/bf02402782.
- [21] V. Kushch, S. Shmegeera, P. Brøndsted, L. Mishnaevsky, Numerical simula-  
tion of progressive debonding in fiber reinforced composite under transverse  
475 loading, *International Journal of Engineering Science* 49 (1) (2011) 17–29.  
doi:10.1016/j.ijengsci.2010.06.020.
- [22] L. P. Canal, C. González, J. Segurado, J. LLorca, Intraply fracture of  
fiber-reinforced composites: Microscopic mechanisms and modeling, *Com-  
posites Science and Technology* 72 (11) (2012) 1223–1232. doi:10.1016/  
480 j.compscitech.2012.04.008.
- [23] L. Bouhala, A. Makradi, S. Belouettar, H. Kiefer-Kamal, P. Frères, Mod-  
elling of failure in long fibres reinforced composites by x-FEM and co-  
hesive zone model, *Composites Part B: Engineering* 55 (2013) 352–361.  
doi:10.1016/j.compositesb.2012.12.013.
- [24] M. Herráez, D. Mora, F. Naya, C. S. Lopes, C. González, J. LLorca,  
485 Transverse cracking of cross-ply laminates: A computational micromechan-  
ics perspective, *Composites Science and Technology* 110 (2015) 196–204.  
doi:10.1016/j.compscitech.2015.02.008.

- [25] L. E. Asp, L. A. Berglund, P. Gudmundson, Effects of a composite-like stress state on the fracture of epoxies, *Composites Science and Technology* 53 (1) (1995) 27–37. doi:10.1016/0266-3538(94)00075-1.
- [26] V. Mantič, Interface crack onset at a circular cylindrical inclusion under a remote transverse tension. application of a coupled stress and energy criterion, *International Journal of Solids and Structures* 46 (6) (2009) 1287–1304. doi:10.1016/j.ijsolstr.2008.10.036.
- [27] R. Krueger, Virtual crack closure technique: History, approach, and applications, *Applied Mechanics Reviews* 57 (2) (2004) 109. doi:10.1115/1.1595677.
- [28] J. R. Rice, A path independent integral and the approximate analysis of strain concentration by notches and cracks, *Journal of Applied Mechanics* 35 (2) (1968) 379. doi:10.1115/1.3601206.
- [29] M. Toya, A crack along the interface of a circular inclusion embedded in an infinite solid, *Journal of the Mechanics and Physics of Solids* 22 (5) (1974) 325–348. doi:10.1016/0022-5096(74)90002-7.
- [30] F. París, J. C. Caño, J. Varna, The fiber-matrix interface crack — a numerical analysis using boundary elements, *International Journal of Fracture* 82 (1) (1996) 11–29. doi:10.1007/bf00017861.
- [31] L. Zhuang, A. Pupurs, J. Varna, R. Talreja, Z. Ayadi, Effects of inter-fiber spacing on fiber-matrix debond crack growth in unidirectional composites under transverse loading, *Composites Part A: Applied Science and Manufacturing* 109 (2018) 463–471. doi:10.1016/j.compositesa.2018.03.031.
- [32] M. Muñoz-Reja, L. Távara, V. Mantič, P. Cornetti, Crack onset and propagation at fibre-matrix elastic interfaces under biaxial loading using finite fracture mechanics, *Composites Part A: Applied Science and Manufacturing* 82 (2016) 267–278. doi:10.1016/j.compositesa.2015.09.023.

- [33] E. Correa, V. Mantič, F. París, Effect of thermal residual stresses on matrix failure under transverse tension at micromechanical level: A numerical and experimental analysis, *Composites Science and Technology* 71 (5) (2011) 622–629. doi:10.1016/j.compscitech.2010.12.027.
- [34] E. Correa, F. París, V. Mantič, Effect of the presence of a secondary transverse load on the inter-fibre failure under tension, *Engineering Fracture Mechanics* 103 (2013) 174–189. doi:10.1016/j.engfracmech.2013.02.026.
- [35] E. Correa, F. París, V. Mantič, Effect of a secondary transverse load on the inter-fibre failure under compression, *Composites Part B: Engineering* 65 (2014) 57–68. doi:10.1016/j.compositesb.2014.01.005.
- [36] C. Sandino, E. Correa, F. París, Numerical analysis of the influence of a nearby fibre on the interface crack growth in composites under transverse tensile load, *Engineering Fracture Mechanics* 168 (2016) 58–75. doi:10.1016/j.engfracmech.2016.01.022.
- [37] C. Sandino, E. Correa, F. París, Interface crack growth under transverse compression: nearby fibre effect, in: *Proceeding of the 18<sup>th</sup> European Conference on Composite Materials (ECCM-18)*, 2018.
- [38] J. Varna, L. Q. Zhuang, A. Pupurs, Z. Ayadi, Growth and interaction of debonds in local clusters of fibers in unidirectional composites during transverse loading, *Key Engineering Materials* 754 (2017) 63–66. doi:10.4028/www.scientific.net/kem.754.63.
- [39] M. Velasco, E. Graciani, L. Távara, E. Correa, F. París, BEM multiscale modelling involving micromechanical damage in fibrous composites, *Engineering Analysis with Boundary Elements* 93 (2018) 1–9. doi:10.1016/j.enganabound.2018.03.012.
- [40] F. París, M. L. Velasco, E. Correa, Micromechanical study on the influence of scale effect in the first stage of damage in composites, *Composites Science*

- and Technology 160 (2018) 1–8. doi:10.1016/j.compscitech.2018.03.004.
- [41] Simulia, Providence, RI, USA, ABAQUS/Standard User’s Manual, Version 6.12 (2012).
- [42] H. Zhang, M. Ericson, J. Varna, L. Berglund, Transverse single-fibre test for interfacial debonding in composites: 1. experimental observations, Composites Part A: Applied Science and Manufacturing 28 (4) (1997) 309–315. doi:10.1016/s1359-835x(96)00123-6.
- [43] L. D. Stasio, J. Varna, Z. Ayadi, Energy release rate of the fiber/matrix interface crack in ud composites under transverse loading: debond-debond and debond-free boundary interactions, submitted to Theoretical and Applied Fracture Mechanics.
- [44] R. Teixeira, S. Pinho, P. Robinson, Thickness-dependence of the translaminar fracture toughness: Experimental study using thin-ply composites, Composites Part A: Applied Science and Manufacturing 90 (2016) 33–44. doi:10.1016/j.compositesa.2016.05.031.
- [45] Z. Hashin, Analysis of composite materials—a survey, Journal of Applied Mechanics 50 (3) (1983) 481. doi:10.1115/1.3167081.
- [46] R. Christensen, K. Lo, Solutions for effective shear properties in three phase sphere and cylinder models, Journal of the Mechanics and Physics of Solids 27 (4) (1979) 315–330. doi:10.1016/0022-5096(79)90032-2.
- [47] F. París, E. Correa, V. Mantič, Kinking of transversal interface cracks between fiber and matrix, Journal of Applied Mechanics 74 (4) (2007) 703. doi:10.1115/1.2711220.
- [48] I. García, V. Mantič, E. Graciani, Debonding at the fibre–matrix interface under remote transverse tension. one debond or two symmetric debonds?, European Journal of Mechanics - A/Solids 53 (2015) 75–88. doi:10.1016/j.euromechsol.2015.02.007.